Journal of Power Sources 216 (2012) 337–344

Contents lists available at SciVerse ScienceDirect

Journal of Power Sources

journal homepage: www.elsevier.com/locate/jpowsour

The influence of channel wettability and geometry on water plug formation and drop location in a proton exchange membrane fuel cell flow field

Alexandru Herescu, Jeffrey S. Allen*

Michigan Technological University, Houghton, MI 49931, USA

HIGHLIGHTS

- We have successfully modeled the minimum volume required to plug a fuel cell channel.
- The effect of degradation of fuel cell components on channel flooding is assessed.
- The utility of Surface Evolver for fuel cell designed has been shown.
- Combinations of bipolar plate and GDL wettabilities can passively move water.

ARTICLE INFO

Article history:
Received 10 January 2012
Received in revised form
10 May 2012
Accepted 16 May 2012
Available online 29 May 2012

Keywords:
PEM fuel cell
Channel flooding
Surface evolver

ABSTRACT

The critical volume of liquid water required to form a plug in a channel having mixed wettability similar to that found in the flow field of a proton exchange membrane (PEM) fuel cell is computed for a range of gas diffusion layer (GDL) and bipolar plate wettabilities and channel bend dihedral angles. Three gas diffusion layers (GDL) with 80, 110 and 150° contact angles are considered while the bipolar plate wettabilities are varied with static contact angles ranging from 50 to 130°. The critical volume is an intrinsic property of the channel-GDL configuration and has direct implications for the liquid holdup, the water distribution in the flow fields of PEM fuel cells as well as on the pumping parasitic power loss. The plug volume correlations may be used as an optimization tool for water management in channels of mixed wettability. The effect of cross-section geometry on the critical volume is also investigated through a comparison between a square and a trapezoidal channel. Mixed wettability drop simulations reveal that water can be passively removed from the GDL surface to the bipolar plate if the latter has a lower contact angle, potentially avoiding the flooding of the porous electrodes.

1. Introduction

Proton Exchange Membrane (PEM) fuel cells convert chemical energy into electrical energy through an electrochemical reaction between hydrogen and air. Protons resulting from the oxidation of hydrogen pass from the anode through a polymeric membrane to the cathode and combine with oxygen to produce water and heat. Catalyst layers on either side of the membrane are required to enable the half-reactions due to the low operating temperature of PEM fuel cells. A single cell of a fuel cell stack is comprised of a porous anode, a proton-conducting membrane, and a porous cathode, the assembly of which is compressed between two plates (bipolar plates) that have embedded gas flow channels to allow for the transport of reactants and water.

A balance must be achieved between water production and removal such that the membrane is hydrated while the passage of gases and water is not obstructed. Water may accumulate in the porous cathode and block the transport of oxygen to the membrane, a condition known as flooding. At high current densities, the production of liquid water may exceed the capacity of the gas streams to remove the water. The resulting decrease in electric potential is known as concentration polarization. Liquid holdup is a condition which occurs when the gas flow channels become completely blocked due to water accumulation and represents an acknowledged barrier to reliable PEM fuel cell development and is the primary motivation for this study. The reader is referred to Bazylak [2], Mukundan and Borup [3], and Trabold et al. [4] for reviews of water visualization and quantification methods, as well as Li et al. [5] in which the water management issues in PEM fuel cell are summarized.

Flooding of the flow fields occurs when liquid drops can no longer be evacuated and sufficient liquid volume accumulates to

* Corresponding author. Tel.: +1 906 487 2349.
E-mail address: jstallen@mtu.edu (J.S. Allen).

0378-7753/$ – see front matter © 2012 Elsevier B.V. All rights reserved.
doi:10.1016/j.jpowsour.2012.05.035

form water plugs. Flow field flooding occurs at relatively low air/H_2 stoichiometry, for which a plug/slug flow regime has been observed in operating fuel cells [6–9]. From microscale two-phase flow studies [10,11] performed in semi-triangular and rectangular microchannels having a hydraulic diameter of 1 mm, it can also be concluded that a plug/slug flow regime is most likely to occur at low gas flow rates that correspond to low stoichiometry ($\leq$2). Two-phase flow regimes in the gas channels and their relevance for the PEM fuel cell operation was reviewed by Anderson et al. [1], who concluded that more optimization work is still needed.

Wetting properties have a significant effect on two-phase flow morphology in a microchannel where gravity is negligible and surface tension is important [12,13]. Wettability is measured by the static contact angle with a 0° indicating a perfectly wetting fluid; that is the fluid spontaneously spreads over a solid surface. A contact angle of 90° is the transition between wetting and non-wetting fluids on a flat surface. The presence of a corner formed by two surfaces presents additional criteria for defining wettability [14]. Liquid can spontaneously wick into or out of a corner due to capillary pressure gradients. The condition under which spontaneous wicking occurs is a combination of corner angle and static contact angle known as the Concus–Finn criteria, $\pi/2 > \alpha + \theta$, where α is the half-angle of the corner and θ is the static contact angle [15]. For the purposes of this discussion, when the channel contact angle for a square cross section is less than 90° but greater than 45° the configuration is considered partially wetting. When, for a square cross section, the contact angle is greater than 90° but less than 135° the configuration is considered partially nonwetting. This designation is based on whether there is an underpressure or overpressure in the water (relative to the gas phase) due to surface curvature. The wetting-nonwetting limits of the channel contact angle (45°, 90°, 135°) will change if the corner angle changes as found in a triangular cross section.

Experiments conducted by Owejan et al. [16] concluded that the effect of flow field channel properties on water accumulation in operational fuel cells are important. They reported that a PTFE coated channel (contact angle $\theta_w = 95°$) demonstrated smaller, more uniformly distributed liquid plugs as compared to an 'uncoated' channel (contact angle $\theta_w = 40°$). Experiments performed by Bazylak et al. [17] reported that partially nonwetting gas channels may enhance drop formation and detachment, at the same time water was not collected under the channel lands. The better performance yielded by the partially nonwetting channels suggests the opportunity of further optimization through surface wettability and geometry. Numerical simulations performed by Ding et al. [18] showed that a less wetting GDL helps in expelling water from its surface while a partially wetting channel increases the GDL water coverage and the water residence time. On the other hand, simulations performed by Cai et al. [19] concluded that partially wetting channels perform better for water discharge and gas diffusion. Quan and Lai [20] reported that for wetting surfaces and edges water transport is facilitated. The enhanced water transport results from corner flow. Ex-situ experiments by Lu et al. [21] reached the conclusion that wetting channels are advantageous over partially wetting or partially nonwetting channels, yielding less flow maldistribution and more stable operation due to a film flow regime. Wetting channels were observed to have draw-backs however, such as enhanced water retention. No general agreement exists for the use of wetting or nonwetting channels and it is clear that more research is necessary to be able to predict the behavior of liquid water in these types of microsystems.

Much of the research on liquid water in the reactant flow fields has been focused on water removal under operating conditions; either experimentally or using computational fluid dynamic (CFD) simulations. A complete review of these studies is beyond the scope of this paper. In general, it is difficult to compare experimental results from different researchers due to subtle differences in cell assembly, operating conditions, and material sets; all of which have a significant effect on water morphology in channels. CFD simulations have attempted to examine the dynamics of plug motion in channels, but have generally been limited to a single plug for which the volume is prescribed due to computational demands and the results remain qualitative [22]. CFD has not been able to predict the size of the plug formed.

Static configuration of liquid water in the flow field for a fuel cell that is not operating can provide useful information on water behavior under the action of capillary forces, at a very modest computational cost. A more thorough understanding of static configuration of water in the flow field will assist in development of material, geometric, and operational strategies for improved water management. Colosqui et al. [23] proposed an analytical method to estimate liquid plug volumes formed under uniform wetting conditions in square acrylic channels. Their observations show that the size of the plug exhibits minimal dependence on the gas and liquid flow rates; indicating that a static calculation of plug volume is appropriate for some fuel cell operating conditions.

Previously, the volume and configuration of a static liquid plug in a fuel cell flow channel was shown to depend on wettability and geometry [24]. The motivation for the study presented herein is to assist the design of gas channels using information on static plug volumes and droplets formed under mixed wetting conditions. The minimum liquid volume required for a plug to exist is investigated. This is similar to recent studies on the stability of drops and plugs in tubes [25,26] and the more general formulation for the existence (and nonexistence) of liquid occlusion in arbitrary tubes under transverse gravitational fields [27]. This study examines the minimum volume required for a plug to exist in channels with planar walls having different wettabilities.

For fuel cell flow fields, the wettability varies between the porous layer and the bipolar plate channel. This mixed wetting between surfaces results in a non-intuitive relationship between water drop location and flow field configuration. Similarly, the relationship between liquid plug formation and volume exhibits unusual behavior based on mixed wettability, channel geometry and channel bends.

2. Computational model

Surface Evolver [28,29] is an experimental mathematics program that can be used to study surfaces that are formed through the action of surface tension as well as other energies. It has been a valuable research tool for applications such as modeling the location of fuel in low gravity, computing capillary surfaces in exotic containers, simulating grain growth, calculating the rheology of foams, modeling the shape of molten solder on microcircuits, studying polymer chain packing, modeling cell membranes, knot energies and classifying minimal surface singularities. There have been limited studies on water morphology in fuel cells using Surface Evolver. The equilibrium morphology of isolated water drops in the porous transport layer with respect to fiber size and orientation has been studied by Roth [30].

Surface Evolver minimizes the total energy, which may have any number of components such as surface tension and gravitational potential. The minimization is performed on an initially defined surface using a gradient descent method. The surface is comprised of triangular facets and the surface energy of a facet is its area multiplied by the surface tension. The contact angle may be set as a constraint after the appropriate edge integral is determined and included in the energy calculation. For a liquid drop sitting on

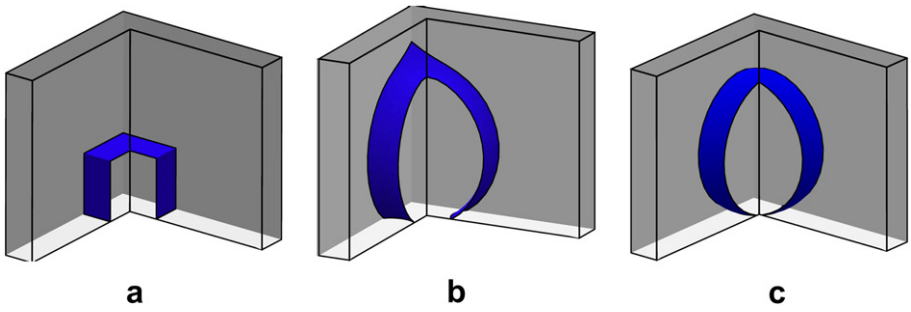

Fig. 1. Initial and converged solutions for liquid that is in contact with the porous electrode (horizontal plane, contact angle θ_b) and two bipolar plate walls (contact angle θ_w) in a channel bend. The drops shown in 1b and 1c are the same volume. (a) Initial model (b) $\theta_b = 150^\circ$ and $\theta_w = 60^\circ$ (c) $\theta_b = 150^\circ$ and $\theta_w = 110^\circ$. (For interpretation of the references to colour in this figure legend, the reader is referred to the web version of this article.)

a plane surface, the contact angle can be implemented by removing the wetted face and assigning to the drop boundary the same energy as that of the removed face. If the wetted face A has an interface energy density T, the energy of the removed plane surface can be ascribed to the contact angle through the corresponding line integral $\int\int_A T\hat{k}\cdot d\mathbf{S} = \int_{\partial A} \mathbf{w}\cdot d\mathbf{l}$, where $\hat{j}$ and $\hat{k}$ are the y and z axes unit vectors. In this case, $\mathbf{w} = xT\hat{j}$ and the corresponding line integral can be included in the total energy as a constraint on the plane surface.

To mimic an actual gas flow channel, the base corresponding to the gas diffusion layer has a contact angle θ_b different from the remaining three walls of the bipolar plate channel which have a contact angle θ_w. The effect of a change in channel wall wettability on drop morphology is shown in Fig. 1 in which the water does not completely plug the channel. The water is in contact with both the vertical walls and the base, but not the channel wall opposite the gas diffusion layer (GDL). An initial configuration is shown in Fig. 1a with the gas–liquid interface in shaded (blue) and the front walls removed for visualization. The contact angle on the horizontal plane (gas-diffusion layer) is the same for both cases with $\theta_b = 150^\circ$. The converged solutions for channel wall contact angles of $\theta_w = 60^\circ$ and 110° are shown in Fig. 1b and c, respectively. The water within a partially wetting channel bend will begin to wick up in the outer vertical corner due to a curvature gradient, while in the partially nonwetting channel bend the water tends to retract out of the corners. A growing drop of water would completely obstruct a partially wetting channel bend earlier than in a partially nonwetting channel bend.

3. Critical plug volume

The critical plug volume V_{CR} is defined as the minimum volume necessary for the water to completely obstruct a channel, that is, to form a plug. V_{CR} is a function of the contact angle, channel cross section and in-plane channel bends. The gravitational potential energy is neglected in the model and the gas–liquid interface shape is determined solely by surface forces. This assumption is justified based on the characteristic length scale of the channel and the resulting Bond number. The Bond number is a ratio of gravitational to capillary effects on the shape of a liquid surface and is defined as $Bo = \rho g L^2/\sigma$, where ρ is the density of the liquid (neglecting the gas density), g is the gravitational acceleration, L is the characteristic length, and σ is surface tension. A water plug in a typical gas flow channel of 0.5 mm hydraulic diameter has $Bo = 0.035$ indicating the gravitational force has minimal effect on the liquid–gas interface shape.

Surface Evolver is only valid for static surfaces even though the surface shape changes with each computational iteration. A moving plug of water would be subject to contact angle hysteresis [31] and viscous stresses so that the interface shape becomes dependent on the flow conditions. Dissipation of energy is not captured in Surface Evolver so dynamic shape and plug volume cannot be studied in this manner. However, static plug interface shape and volume characterize intrinsic properties of mixed wettability channels and are a good indicator of the anticipated liquid water distribution in the reactant flow channels at low air/H_2 stoichiometry. In addition, the frequency of plug formation can be estimated for a given current density when the reactant flow is fully saturated.

The critical plug volume is determined by iteratively changing the volume of the initial model, shown in Fig. 2. Each converged solution is computed by solving for a minimum energy interface with boundary conditions θ_b and θ_w in a channel with dihedral 2α, where $2\alpha = 180^\circ$ is a straight channel. The surface defining the plug end translates during a Surface Evolver run and reaches a position according to the prescribed volume. The critical volume solution is determined when the ends of the liquid plug intersect resulting in a singularity. The critical volume calculated is the minimum volume for which a plug will exist. This volume is not the same as that determined using the stability limit of a growing drop that eventually forms a plug [25]. The critical volume is an intrinsic property of the mixed wettability channel whereas the plug volume determined by the stability of a growing drop will depend on the location of the drop; i.e. on the channel surface, on the GDL, or in a corner.

A Surface Evolver run requires modest computational time. Using an IBM T60 notebook with an Intel Centrino Duo T2500 CPU at 2 GHz and 512 MB of RAM, a minimum energy surface is obtained in 5–10 min. The geometric and surface energy constraints (facet energies) are checked for consistency by solving for a volume with 90° contact angles resulting in flat interfaces. This provides an easy visual validation of the input model as well as a check on volume calculation.

In Fig. 2 the initial model is shown for a volume of water sufficient to plug the channel. Only half of a plug is shown, the other half being

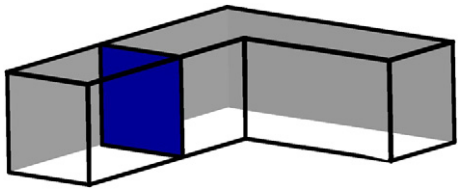

Fig. 2. Initial model for determining the critical volume of a plug in a bend of a square channel using Surface Evolver. The left plug end consisting of a gas/water interface is shown, the right end (not visible) is symmetrically disposed. (For interpretation of the references to colour in this figure legend, the reader is referred to the web version of this article.)

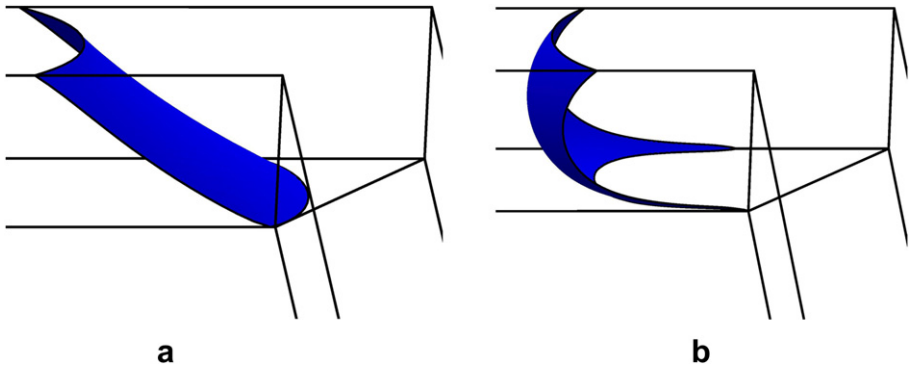

Fig. 3. Critical volume plug in a 90° bend of a square channel for $\theta_b = 150°$ on the GDL surface (lower horizontal plane). The interface curvature is positive for $\theta_w = 50°$ on the bipolar plate (vertical planes and upper surface) and the water is in a state of under-pressure with respect to the gas. For the nonwetting cases the curvature is negative with the water in a state of over-pressure with respect to the gas. (a) $\theta_w = 50°$ (b) $\theta_w = 130°$.

symmetric with respect to the bend dihedral bisector. The gas–liquid interface that forms the left plug side is shown shaded (blue). The value of surface tension is set to one, which is valid for a Bond number of zero. Changing the value of surface tension would subsequently change the line integral value corresponding to the contact angle. Therefore, changing the value of surface tension will have no effect on the converged interface shape nor the critical volume. Inclusion of gravitational potential would necessitate incorporation of scaled forces through the Bond number. The converged solutions for a GDL wettability of $\theta_b = 150°$ and two channel wettability conditions in a 1×1 cross section are shown in Fig. 3. The critical plug volume for these runs are 2.16 and 3.52 for channel wall contact angles of $\theta_w = 50°$ and $\theta_w = 130°$, respectively. A plug of a lesser volume cannot exist in this configuration. The critical volume in a $d \times d$ square channel cross section can be obtained by multiplying V_{CR} by d^3.

The interface curvature and the critical plug volume change with surface wettability. The $\theta_w = 50°$ plug has a positive interface curvature with liquid pressure less than gas pressure, while the $\theta_w = 130°$ plug has negative curvature with liquid pressure higher than the gas. Values of θ_w below 45° cannot be simulated because a solution does not exist or is unbounded per the Concus–Finn criterion [15], which is the criteria for capillary wicking in a corner. For $\theta_w = 50°$ the liquid plug is stretched along the upper corners as the Concus–Finn criteria of 45° is approached. If the contact angle on the channel surface is below 45°, the liquid could spread spontaneously along the corner thereby draining the plug [32,33]. Thus, the lower limit for a converged solution is set by the Concus–Finn criterion, and the lowest wall contact angle used is 50° in order to attain convergence.

Contact angles below 45° would favor a relatively stable configuration corresponding to a liquid film attached to the more wetting surface as observed experimentally [21]. For partially nonwetting surfaces as shown in Fig. 3b the liquid begins to de-wet the corners. This effect may occur when the contact angle is greater than 90° for perpendicular faces and will become more pronounced as the contact angle increases. A bounded solution does not exist for a channel with perpendicular walls when the contact angle approaches $\theta_w = 135°$. At 135°, the liquid will tend to spontaneously evacuate the corners in the absence of any other forces, but that does not preclude plug formation in fuel cell flow fields.

Figs. 4 and 5 show the dependency of critical volume on contact angles and bend dihedrals. Critical volume solutions for a fixed GDL contact angle ($\theta_b = 110°$) and four bend dihedrals are shown for a range of bipolar plate wall contact angles (θ_w) in Fig. 4. A similar data set for $\theta_b = 150°$ is shown in Fig. 5. Each data point represents a fully converged solution.

The critical volume solutions in a square cross section exhibit similar trends with respect to wall contact angle θ_w. The data set for each bend dihedral is offset from the straight channel by 1/tan (α), where α is the half-angle of the bend. Therefore, a correlation for V_{CR} as a function of θ_w can be generated for all bend dihedrals.

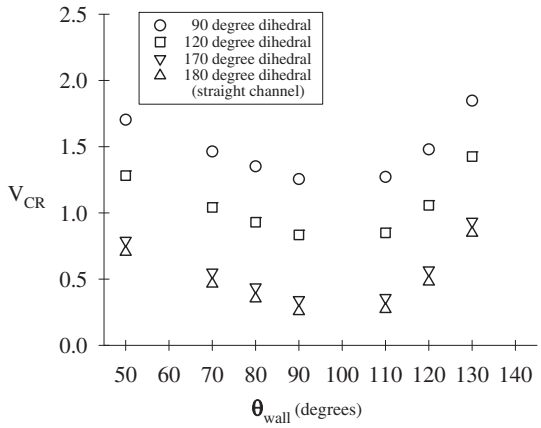

Fig. 4. Critical plug volume in a 1×1 square channel for a range of bipolar plate contact angles θ_w for bend dihedral angles of 90°, 120°, 170° and 180° (straight channel). The base, or GDL, contact angle is $\theta_b = 110°$.

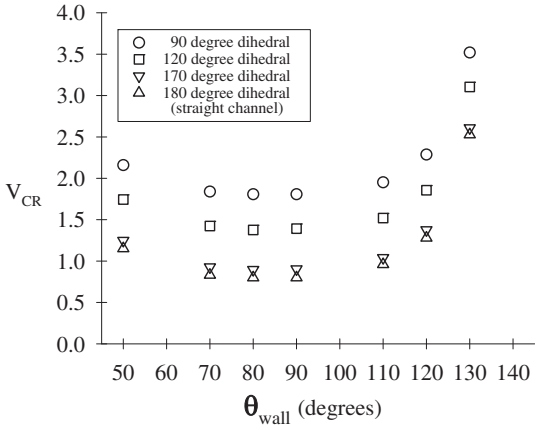

Fig. 5. Critical plug volume in a 1×1 square channel for a range of bipolar plate contact angles θ_w for bend dihedral angles of 90°, 120°, 170°, and 180° (straight channel). The base, or GDL, contact angle is $\theta_b = 150°$.

Table 1
V_{CR} correlation coefficients for a 1 × 1 square cross section channel with a contact angle θ_b on the GDL side. All angles are in degrees. The correlation for $\theta_b = 110°$ condenses all of the data shown in Fig. 4 to a single curve. Similarly, the correlation for $\theta_b = 150°$ condenses all of the data shown in Fig. 5. The correlation for the trapezoidal section is only valid for a straight channel, for which the last term of equation (1) is 0. The correlation coefficients are for θ_w in degrees and normalized by 90°.

	$\grave{e}_b$	a_0	a_1	a_2	a_3	a_4	r^2
Square	80	−0.3910	5.0443	−11.5088	8.8721	−1.9562	0.9983
Square	110	0.8868	−0.0233	0.4513	−2.7382	1.6787	0.9995
Square	150	21.6526	−93.2994	154.7584	−112.7123	30.4181	0.9952
Trapezoidal	110	4.7701	−16.4804	28.052	−23.9858	7.9031	0.9988

$$V_{CR} = a_0 + a_1\left(\frac{\theta_w}{90}\right) + a_2\left(\frac{\theta_w}{90}\right)^2 + a_3\left(\frac{\theta_w}{90}\right)^3 + a_4\left(\frac{\theta_w}{90}\right)^4 + \frac{1}{\tan(\alpha)} \quad (1)$$

where a_i are fitting coefficients and θ_w is in degrees. The coefficients a are given in Table 1 for base contact angles of 80°, 110° and 150°. The correlations are valid for wall contact angles of $50° \leq \theta_w \leq 130°$ and bend dihedrals from 90° to 180°. For $2\alpha = 180°$ the channel is straight (without bend) and last term of the correlation is set to zero.

The dependence of these correlation on the GDL contact angle is not simple and a separate correlation for each θ_b appears to be necessary. Fig. 6 shows the correlation for three different base contact angles (80°, 110°, and 150°) and a wall contact angle between $50° \leq \theta_w \leq 130°$ in a 1 × 1 channel. The dihedral angle factor of 1/tan (α) has been subtracted from each simulation so that the correlation is, in effect, for the straight channel. If the contact angle on the GDL surface decreases there is also a trend of decreased critical plug volumes, though not uniformly with channel contact angle. An example can be seen in the intersection of 80° and 110° correlations in Fig. 6. The relative change in critical volume is not intuitive and indicates the need for specific simulations when wetting and nonwetting GDLs are used. For this particular case the critical volume is larger for the 80° GDL when the bipolar plate contact angle θ_w is greater than 102°.

The general trend in critical volume correlations shown in Fig. 6 can be separated into partially nonwetting ($1 < \theta_w/90° < 1.5$) and partially wetting ($0.5 < \theta_w/90° < 1$) interior corners. The critical volume increases as the wall contact angle approaches the convergence limits of 45° and 135° ($0.5 < \theta_w/90° < 1.5$), though the rate of increase in critical volume is much greater on the partially nonwetting side of the correlation. A gross estimate of plug length can be inferred from the value of the critical volume, $V_{CR} \sim L/d$, where L is the plug length and d is the hydraulic diameter of the channel. The exact length will depend upon the meniscus curvature. Thus, per Fig. 6, the plug length is approximately 2.5 times the channel dimension for $\theta_b = 150°$, $\theta_w/90° = 1.4$ and approximately 0.5 times the channel dimension for $\theta_b = 110°$, $\theta_w/90° = 1.4$. The plug length corresponding to the critical volume is always less than three channel dimensions for the square cross section. Based on these correlations a channel-GDL configuration could be designed to deliver liquid plugs of a specific (critical) volume, which prompts the question of which critical volume (small or large) is most advantageous for fuel cell operation.

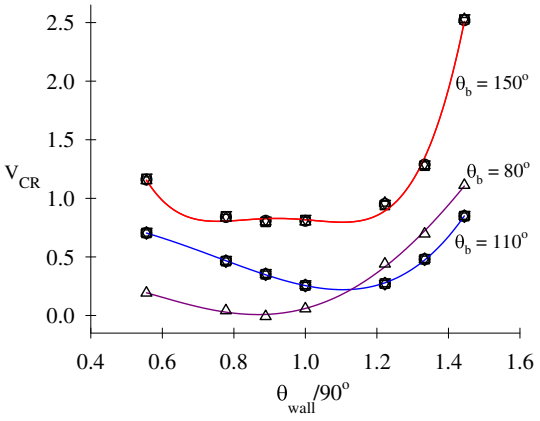

Fig. 6. Critical plug volume in 1 × 1 square channels for a range of bipolar plate channel contact angles θ_w, three values of θ_b corresponding to three different GDLs. The correlations shown (solid lines) correspond to equation (1) and Table 1 for the straight ($2\alpha = 180°$) channel. The family of curves shown in Figs. 4 and 5 are obtained by adding 1/tan (α).

Experimental observations indicate that a single large plug is easier to move than multiple small plugs through a capillary-scale channel comparable to fuel cell flow fields [34]. This observation is generally true when the static contact angles range from 60° to 130° for which the energy dissipation resulting from moving contact lines is an important mechanism resisting plug motion [35]. Lee and Lee [36] note that pressure drop for plug flow in polyurethane and teflon tubes decreases with a reduction in the number of moving plugs. A follow on study concluded that the moving contact lines are a major factor in determining the pressure drop of plug flow [37]. Based on these experimental studies, for fuel cell operating conditions during which plug formation occurs, the flow field can more easily be cleared for lower frequency plug formation (longer average plug lengths). The channel-GDL surface energies that result in the longest plug length is for the partially nonwetting conditions as shown in Figs. 4–6.

The experimental study by Owejan et al. [16], which examined plug formation in an operating fuel cell under various channel wettabilities, would seem to contradict this conclusion. Their results show that the partially nonwetting channels ($\theta_w = 95°$) exhibited small, more uniformly distributed plugs than the wetting channels ($\theta_w = 40°$). Also, the partially nonwetting channels ($\theta_w = 95°$) demonstrated better performance in the mass transport limited region of the polarization curve as compared to the wetting channels; i.e., better performance with small plug lengths rather than long plug lengths. However, a channel contact angle of 40° meets the Concus–Finn criteria in both the square and triangular cross sections tested. This results in liquid accumulation along the channel corners so that when a plug forms, the length can be on the order of a hundred hydraulic diameters as shown in neutron images. Under these conditions the inertial resistance impeding the motion of the plug becomes important in addition to the contact line energy dissipation. The wetting conditions ($\theta_w = 40°$) in the study by Owejan et al. [16] do not allow for a bounded solution using Surface Evolver because of corner wicking. For moderate length plugs that are less than three hydraulic diameters as predicted using Surface Evolver, contact line dissipation will be the dominant mechanism resisting plug motion. The fewer the contact lines, the easier the plugs can be removed from the flow field.

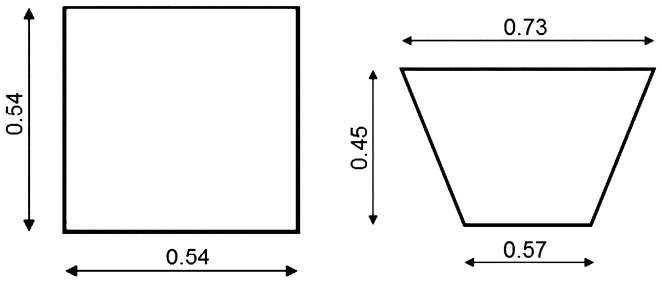

Fig. 7. Square and trapezoidal cross sectional areas used for comparison of critical volumes. The area of the two sections are both 0.2925 mm^2.

3.1. Comparison of critical volume for square and trapezoidal cross sections

The critical volume is compared for a square and a trapezoidal cross section with dimensions used in a typical PEM fuel cell flow field. The isosceles trapezoidal channel having the parallel sides of 0.57 and 0.73 distanced by 0.45 with a cross-sectional area of 0.2925 mm^2 has the same cross sectional area as a square channel of width 0.5408 mm. Fig. 7 illustrates the respective geometries. The critical volume analysis enables a comparison between the square and trapezoidal geometries under varied wetting conditions.

Fig. 8 is a comparison of critical volume for the square and trapezoidal cross sections for a 180° degree bend dihedral (straight channel) with a GDL contact angle of $\theta_b = 110°$. A simple relationship for the bend dihedral has not been found for the trapezoidal cross section. Thus, the trapezoidal correlation expressed in equation (1) with the coefficients listed in Table 1 are only for a straight channel. For a geometrically similar trapezoidal section with parallel sides spaced by a distance ℓ, the critical volume can be obtained from multiplying equation (1) by $(\ell/0.45)^3$.

In a straight channel the critical volume V_{CR} is larger for the trapezoidal section than for the square section when $\theta_w \geq 110°$ even though the cross sectional areas are the same. At $\theta_w = 120°$, the trapezoidal critical volume is 20% greater and is 50% greater at $\theta_w = 130°$. The implication is that the larger the critical volume, the less frequently plug formation will occur under nominal fuel cell operating conditions and the less pressure drop required to keep the channels clear of water. Lu et al. [21] did not observe a significant difference in pressure drops for plug flow in square and trapezoidal cross sections with the same dimensions shown in Fig. 7. However, the channel contact angle is reported as 85°, which per Fig. 8 should result in nearly identical critical volumes and subsequently, similar plug lengths.

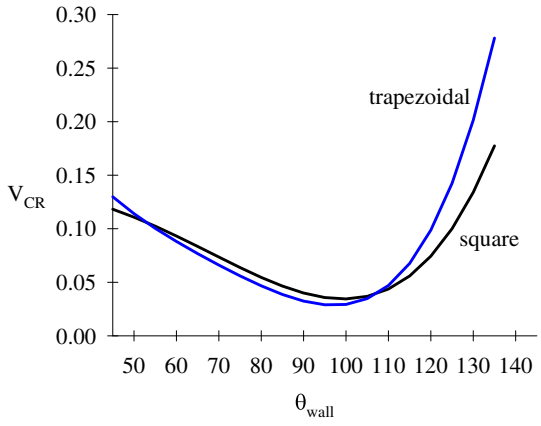

Fig. 8. Liquid hold-up in a straight channel, square 0.54 × 0.54 and trapezoidal sections with parallel sides of 0.57 and 0.73 spaced by 0.45 as illustrated in Fig. 7. The GDL contact angle is $\theta_b = 110°$ and the bipolar plate contact angle θ_w is varied. The curves shown are correlations per equation (1).

3.2. Plug formation frequency

The time required for a sufficient volume of water to accumulate for plug formation can be approximated using the critical volume. The calculation assumes that water is collected over a channel length equal to three hydraulic diameters roughly approximating the Rayleigh instability wavelength, which has been shown as a valid pinch-off wavelength for capillary-scale two-phase flows [38–43]. For a liquid water flux into the cathode flow field at an equivalent current density of 0.4 cm^{-2} over an active area of 18.4 cm^2, similar to the ex-situ experiments performed by Lu et al. [7], the time necessary for critical volume accumulation may vary significantly between the trapezoidal and square cross sections depending on the channel contact angle. When $\theta_b = 110°$ and $\theta_w = 130°$, the time to critical volume is 140 s in the square section, while in the trapezoidal section the time is 211 s.

4. Drop location as a result of mixed wettability

Even though water is uniformly distributed along the channels for high V_{CR} values, the cross-sectional water distribution may be predominantly towards the GDL. This implies that the gas transport across the GDL would be blocked resulting in flooding of the porous electrodes. Capillary forces naturally present in microchannels pose a challenge for water transport due to a large area-to-volume ratio. Surface Evolver simulations were performed for drops being in contact with two adjacent walls of a rectangular channel having different wettabilities simulating a water drop simultaneously contacting the bipolar plate and GDL.

The case of a drop which forms on the GDL side and makes contact with one of the bipolar plate walls is shown in Fig. 9. The GDL has $\theta_b = 150°$ (horizontal plane) and the bipolar plate has $\theta_w = 100°$ (vertical plane). The drop shape and location is solely dictated by capillary forces that are initially unbalanced due to the difference in the surface energies of the two walls. The surface tension forces act on the drop surface as well as on the contact lines which are present at the gas/liquid/solid junction. The contact angle on the walls was prescribed and the drop evolution is shown at different iteration steps in Fig. 9. The liquid volume migrates towards the lower contact angle surface, which is the vertical wall in order to minimize the surface area under given contact angles. This implies that water can be passively removed from the GDL surface to the bipolar plate walls by sole means of capillary forces, preventing thus the blockage of gas transport through the porous electrodes as well as flooding. Experimental observations of Bazylak et al. [17] corroborate this result.

5. Wetting or nonwetting channels?

In order to better predict the flow morphology for preliminary design purposes, the critical volume data has to be corroborated with other information concerning either the particular geometry such as the presence of bends, the existence and stability of liquid films, and the presence of moving contact lines. For example, a GDL with $\theta_b = 150°$ can have the same critical volume with either a partially wetting channel ($\theta_w = 60°$) or a partially

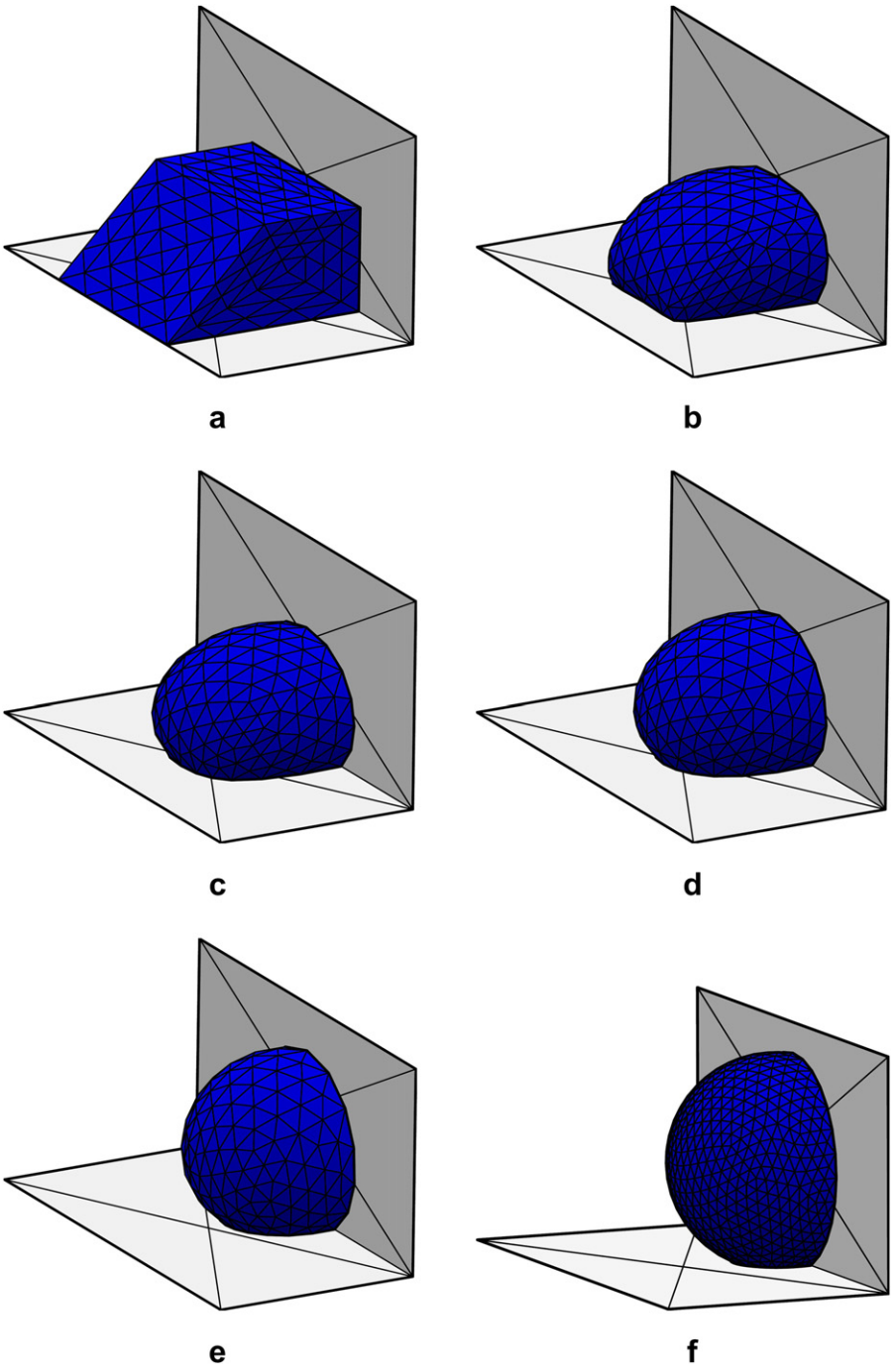

Fig. 9. Energy minimization steps towards an equilibrium configuration (*f*). The base (GDL) contact angle is $\theta_b = 150^\circ$ and the channel wall contact angel is $\theta_w = 100^\circ$.

nonwetting wall ($\theta_w = 110^\circ$) as shown in Fig. 6. The choice of partially wetting or partially nonwetting channels is not immediately obvious. If other channel features such as bends are present, then additional simulations can be used to help determine the more optimal wetting condition. The channel bend simulations shown in Fig. 1 indicate that the partially wetting channel ($\theta_w = 60^\circ$) would tend to plug earlier than the partially nonwetting ($\theta_w = 110^\circ$) channel for a drop growing in the bend. Therefore, the partially nonwetting channel would appear to be the more optimal configuration. Each combination of channel geometry, channel wettability, and GDL wettability presents a unique scenario.

Degradation of the GDL often results in a lower θ_b [44] and this may negatively impact fuel cell performance by decreasing V_{CR}, resulting in more numerous plugs. Using the correlations shown in equation (1) and Table 1, if a square channel with an initial GDL contact angle of 150° and channel contact angle of $\theta_w = 100^\circ$ degrades to $\theta_b = 80^\circ$ and $\theta_w = 80^\circ$, then the critical plug volume will decrease by nearly a factor of ten. Ten times less water would be required to plug the degraded channel resulting in many more liquid plugs for a given current density. Consequently, there will be many more moving contact lines within the same channel length and clearing the channel will be more difficult as compared to the initial wetting conditions.

6. Conclusion

The critical volume calculations via Surface Evolver enable estimation of the minimum volume of water required to plug the flow field channel of a PEM fuel cell with mixed wettability between the bipolar plate and the GDL. The correlations for critical volume are sensitive to the GDL and channel contact angles as well as channel cross-section and channel bends. For square cross section channels, the bend dihedral can be accounted for in the correlations of V_{CR} and θ_w through a single term, 1/tan (α). The utility of Surface Evolver has also been demonstrated with determining the equilibrium location of discrete drops within a fuel cell flow field. Notably, simulations show that water can be passively removed from the GDL surface to the bipolar plate if the latter has a lower contact angle, potentially avoiding flooding of the GDL.

The critical volume represents an intrinsic property of mixed wettability channels and V_{CR} is an implicit measure of static plug formation. As such, the magnitude of the critical volume can be used to estimate the frequency of plug formation during fuel cell operation at low reactant flow rates. Though the calculated critical volumes are for static morphologies, the effect of component degradation on water management can be inferred. The calculated critical volumes with corresponding correlations can be used to assess the effect of material degradation on water accumulation in flow field channels.

Partially nonwetting channels will tend to form relatively large plugs as compared to partially wetting channels, though the difference is only significant at the upper end of nonwetting. At $\theta_w > 120^\circ$ the divergence in V_{CR} becomes apparent. This range of channel wettability would tend to produce the least number of liquid plugs, with the least number of moving contact lines. Experimental observations and energy dissipation arguments suggest that relatively large partially nonwetting plugs would be advantageous for fuel cell operation. Unfortunately, there appears to be no experimental data available for fuel cell operation with channel wettabilities greater than 120°. Contact angles on materials used for bipolar plates generally range from 80° to 120°, which exhibit small variations in critical volume as shown in Figs. 4–6. Fuel cell testing with $\theta_w > 120^\circ$ would provide valuable results that could be used to assess the effectiveness of highly nonwetting GDL-channel combinations on water management in the flow field.

Acknowledgement

This work was sponsored by the U.S. Department of Energy under contract DE-FG36-07GO17018 and by the Department of Mechanical Engineering – Engineering Mechanics at Michigan Technological University in collaboration with the Rochester Institute of Technology and General Motors. A. Herescu is indebted to the DeVlieg Foundation and its support for diverse research in ecological technologies. He also expresses his gratitude to the Graduate School at Michigan Technological University for the support granted through a Doctoral Finishing Fellowship.

References

[1] R. Anderson, L. Zhang, Y. Ding, M. Blanco, X. Bi, D.P. Wilkinson, Journal of Power Sources 195 (15) (2010) 4531–4553.
[2] A. Bazylak, International Journal of Hydrogen Energy 34 (9) (2009) 3845–3857.
[3] R. Mukundan, R.L. Borup, Fuel Cells 9 (5) (2009) 499–505.
[4] T.A. Trabold, J.P. Owejan, J.J. Gagliardo, D.L. Jacobson, D.S. Hussey, M. Arif, Use of Neutron Imaging for Proton Exchange Membrane Fuel Cell (PEMFC) Performance Analysis and Design, John Wiley & Sons, Ltd, 2009, pp. 1–15, (chapter 44).
[5] H. Li, Y. Tang, Z. Wang, Z. Shi, S. Wu, D. Song, J. Zhang, K. Fatih, J. Zhang, H. Wang, Z. Liu, R. Abouatallah, A. Mazza, Journal of Power Sources 178 (1) (2008) 103–117.
[6] I.S. Hussaini, C.-Y. Wang, Journal of Power Sources 187 (2) (2009) 444–451.
[7] Z. Lu, S.G. Kandlikar, C. Rath, M. Grimm, W. Domigan, A.D. White, M. Hardbarger, J.P. Owejan, T.A. Trabold, International Journal of Hydrogen Energy 34 (8) (2009) 3445–3456.
[8] L. Yu, W. Chen, M. Qin, G. Ren, Journal of Power Sources 189 (2) (2009) 882–887.
[9] J.P. Owejan, J.J. Gagliardo, J.M. Sergi, S.G. Kandlikar, T.A. Trabold, International Journal of Hydrogen Energy 34 (8) (2009) 3436–3444.
[10] K.A. Triplett, S.M. Ghiaasiaan, S.I. Abdel-Khalik, D.L. Sadowski, International Journal of Multiphase Flow 25 (3) (1999) 377–394.
[11] W. Qu, S.-M. Yoon, I. Mudawar, Two-phase flow and heat transfer in rectangular micro-channels. Proceedings of the ASME Summer Heat Transfer Conference, pp. 397–410, Las Vegas, NV, United States, 2003.
[12] A.B. Barajas, R.L. Panton, International Journal of Multiphase Flow 19 (2) (1993) 337–346.
[13] S. Y. Son, J. S. Allen, Visualization and Predictive Modeling of Two-Phase Flow Regime Transition with Application Towards Water Management in the Gas-Flow Channels of PEM Fuel Cells. *IMECE2005-82422*, 2005 ASME International Mechanical Engineering Congress & Exposition, Orlando, Florida, November 5–11 2005.
[14] J.S. Allen, S.Y. Son, S.H. Collicott, Handbook of Fuel Cells: Advances in Electrocatalysis, Materials, Diagnostics and Durability. In: W. Vielstich, H.A. Gasteiger, H. Yokokawa (Ed.), vol. 6, John Wiley & Sons Ltd, Chichester, UK, pp 687–698.
[15] P. Concus, R. Finn, Proceedings of the National Academy of Sciences of the United States of America 63 (2) (1969) 292–299.
[16] J.P. Owejan, T.A. Trabold, D.L. Jacobson, M. Arif, S.G. Kandlikar, International Journal of Hydrogen Energy 32 (2007) 4489–4502 (Compendex).
[17] A. Bazylak, J. Heinrich, N. Djilali, D. Sinton, Journal of Power Sources 185 (2) (2008) 1147–1153.
[18] Y. Ding, H.T. Bi, D.P. Wilkinson, Journal of Power Sources 196 (15) (2011) 6284–6292.
[19] Y.H. Cai, J. Hu, H.P. Ma, B.L. Yi, H.M. Zhang, Journal of Power Sources 161 (2) (2006) 843–848.
[20] P. Quan, M.-C. Lai, Journal of Power Sources 164 (1) (2007) 222–237.
[21] Z. Lu, C. Rath, G. Zhang, S.G. Kandlikar, International Journal of Hydrogen Energy 36 (16) (2011) 9864–9875.
[22] A. Mukherjee, J. S. Allen, Numerical Study Of Liquid Slug Stability During Adiabatic Two Phase Flow Inside A Minichannel. IMECE2007-43418, 2007 ASME International Mechanical Engineering Congress and Exposition, Seattle, Washington, USA, November 11–15, 2007.
[23] C.E. Colosqui, M.J. Cheah, I.G. Kevrekidis, J.B. Benziger, Journal of Power Sources 196 (23) (2011) 10057–10068.
[24] A. Herescu, J.S. Allen, ECS Transactions 26 (1) (2010) 219–225.
[25] S.H. Collicott, J. P. Braun, Stability of Droplets and Bubbles in a Bent Tube. 44th AIAA Aerospace Sciences Meeting, Reno, NV, 2006.
[26] S.H. Collicott, W.G. Lindsley, D.G. Frazer, Physics of Fluids 18 (8) (2006) 087109.
[27] R. Manning, S. Collicott, R. Finn, Journal of Fluid Mechanics 682 (2011) 397–414.
[28] K. Brakke, Experimental Mathematics 1 (2) (1992) 141–165.
[29] K. Brakke, Surface Evolver, Ver. 2.14 (2003).
[30] J. Roth, Water Transport in Gas Diffusion Media for PEM Fuel Cells: Experimental and Numerical Investigation. PhD thesis, Universität Duisburg-Essen, 2010.
[31] E.B. Dussan V, Annual Review of Fluid Mechanics 11 (1979) 371–400.
[32] M.M. Weislogel, S. Lichter, Journal of Fluid Mechanics 373 (1998) 349–378.
[33] M.M. Weislogel, C. Nardin, Microgravity Science and Technology XVII (3) (2005) 45–55.
[34] E. Kimball, T. Whitaker, Y.G. Kevrekidis, J.B. Benzinger, AIChE Journal 54 (5) (2008) 1313–1332.
[35] P.G. De Gennes, F. Brochard-Wyart, D. Quere, A. Reisinger, Capillarity and Wetting Phenomena: Drops, Bubbles, Pearls, Waves, Springer Verlag, 2004.
[36] C.Y. Lee, S.Y. Lee, Experimental Thermal and Fluid Science 32 (8) (2008) 1716–1722.
[37] C.Y. Lee, S.Y. Lee, Experimental Thermal and Fluid Science 34 (1) (2010) 1–9.
[38] P.S. Hammond, Journal of Fluid Mechanics 137 (1983) 363–384.
[39] T.C. Ransohoff, P.A. Gauglitz, C.J. Radke, AIChE Journal 33 (5) (1987) 753–765.
[40] S.L. Goren, Journal of Fluid Mechanics 12 (1963) 309–319.
[41] H.H. Hu, D.D. Joseph, Journal of Fluid Mechanics 205 (1989) 359–396.
[42] P.A. Gauglitz, C.J. Radke, Journal of Colloid and Interface Science 134 (1) (1990) 14–40.
[43] D.H. Everett, J.M. Haynes, Journal of Colloid and Interface Science 38 (1) (1972) 125–137.
[44] F.A. de Bruijn, V.A.T. Dam, G.J.M. Janssen, Fuel Cells 8 (1) (2008) 3–22.